

A Thermodynamic Model for Argon Plasma Kernel Formation

Kian Eisazadeh-Far¹, Farzan Parsinejad², Hameed Metghalchi^{1*}
James C. Keck³

¹Northeastern University, Mechanical and Industrial engineering Department, Boston, MA 02115

²Chevron Oronite Company LLC, Richmond, CA 94801

³Massachusetts Institute of Technology, Cambridge, MA 02139

metghalchi@coe.neu.edu

Abstract

Plasma kernel formation of argon is studied experimentally and theoretically. The experiments have been performed in a constant volume cylindrical vessel located in a shadowgraph system. The experiments have been done at constant pressure. The energy of plasma is supplied by an ignition system using two electrodes located in the vessel. The experiments have been done with two different spark energies to study the effect of input energy on kernel growth and its properties. A thermodynamic model employing mass and energy balances was developed to predict the experimental data. The agreement between the experiments and model prediction is very good. The effect of various parameters such as initial temperature, initial radius of the kernel, and the radiation loss have been investigated and it has been concluded that the initial condition is very important on the formation and expansion of the kernel.

Keywords: Argon plasma; kernel formation; thermodynamic model; ionization.

1. Introduction

Since plasma kernel formation is the beginning of flame propagation in many systems, understanding this process is very important. In plasma kernel formation of a non-combustible gas by an external energy source like a spark, there are two important processes: The first part which is very short (microseconds) is the formation of a spark channel between two electrodes. The second part which is longer (milliseconds) is the conversion of electrical energy to thermal energy and consequently ionization and plasma kernel expansion. In the case of the existence of a combustible gas, the third stage will be evolution of the plasma kernel to a self sustained flame.

There are numerous theoretical and experimental studies on the first and third stages (Bradley et al., 2004; Kravchik & Sher, 1994; Lee et al., 2000; Maly, 1981; Mantel, 1992; Pischinger & Heywood, 1991; Sher & Keck, 1986; Sher et al., 1992; Yossefi et al., 1993; Ziegler et al., 1985). Maly and Vogel (1979) in a theoretical and experimental study determined that the most important part of spark discharge is the breakdown process. They mentioned that the other processes including arc and glow discharge are less important because their electrical energy is dissipated into the electrodes. Sher et al (1992) did a fundamental study on spark formation in air and proposed a model to calculate the spark kernel temperature after breakdown. They concluded that the initial spark kernel is a very high temperature region, but the temperature drops rapidly due to energy dissipation. They stated that beyond a specific limit of temperature, the energy of spark affects the flame kernel size, and not the temperature. They concluded that the spark kernel is grown in two steps. The first, shorter stage consists of a pressure wave emission. This is followed by a

longer period, in which constant pressure ionization starts. Chen and Ju (2007) studied the evolution of the ignition kernel to a flame ball and they concluded that radiation plays a very important role in transition of initial flame kernel to the actual self-sustained flame.

Most of the cited studies focus on the first and third stage of ignition and a semi-quantitative understanding of these stages has been achieved. In this paper we will focus on the second part of ignition which is the formation and expansion of the plasma kernel by adding electrical energy. We will study the plasma kernel of an inert gas, argon, to avoid the complexities of a reacting gas mixture and multi-component species.

2. Experimental System

Figure 1 shows the sketch of the experimental system. The experimental system includes a cylindrical vessel. It is fitted with two extended spark plug electrodes which provide a central point ignition source for the chamber. The thickness of electrode (de) is 0.381 mm. A shadowgraph system is used with the cylindrical system to take images of kernel growth. A CMOS camera with the capability of taking pictures up to 40,000 frames per second has been used in these experiments. Additional information about the experimental facility can be found in previous publications (Eisazadeh-Far, Moghaddas, Al-Mulki, & Metghalchi, 2010; Eisazadeh-Far, Parsinejad, & Metghalchi, 2010; Eisazadeh-Far, Parsinejad, Metghalchi, & Keck, 2010; Parsinejad, Arcari, & Metghalchi, 2006; Parsinejad, Keck, & Metghalchi, 2007; Rahim, Eisazadeh-Far, Parsinejad, Andrews, & Metghalchi, 2008).

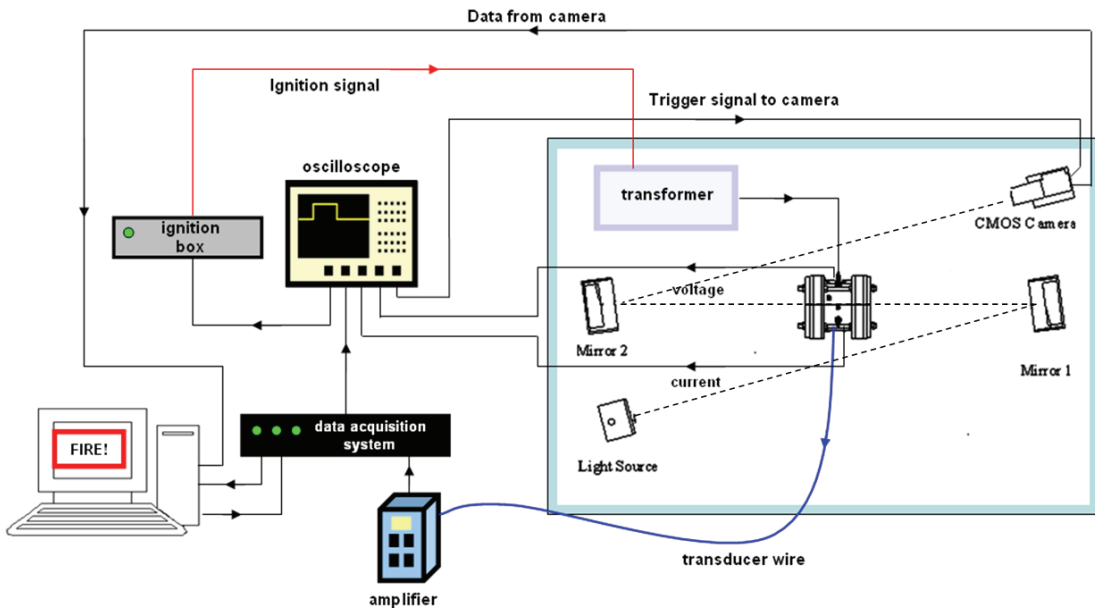


Figure 1: The experimental set up of the system.

Ignition system: An important detail of the ignition system is the 5 select-switch, which allows the energy stored in the capacitors to be varied. The capacitors storing this energy discharge to a transformer and therefore to spark plugs. Voltage and current across the spark plug gap during the electrical discharge have been measured to calculate the discharge energy. This has been achieved by setting up a detection circuit employing two resistors. The resistors are placed in parallel to the spark plugs to allow only a very small but measurable portion of the current to flow through the detection circuit. These small portions were then sampled by an oscilloscope. In this system the voltage difference across one of the resistors in the detection circuit is 1/201 of the voltage across the spark plugs. Another similar method was used to calculate the current across the spark plug, which in this case is exactly equal to the amperage flowing through the parallel circuit.

3. Experimental Results

3.1. Discharge energy (DE): Using a voltage divider circuit, the voltage and current across the gap were measured. Figure 2 shows the experimentally determined voltages and currents across the spark plug gap for each voltage setting on the ignition system in argon. The spike, approximately at 5-10 microseconds in duration, shows the breakdown stage which is the beginning of spark discharge. In this stage the gap is bridged by the avalanche of electrons flowing from cathode to anode.

Figure 3 shows the discharged power calculated by the product of the measured values of current (I) and voltage (V) for two different stored energies in the ignition system. Discharged energy, DE, can be calculated as $DE = \int VI dt$. It should be noted that discharged energy is different from the electrical energy converted to the thermal energy in the gas. A portion of the discharged energy is dissipated by conduction into the electrodes.

3.2. Image capturing: Figures 4 shows the snapshot of an argon plasma kernel. It can be seen that the boundary layer surrounding the plasma kernel is very thin. Figure 5 shows the radii of a kernel at two different spark energies. It can be seen that spark energy has a remarkable effect on the size of the kernel.

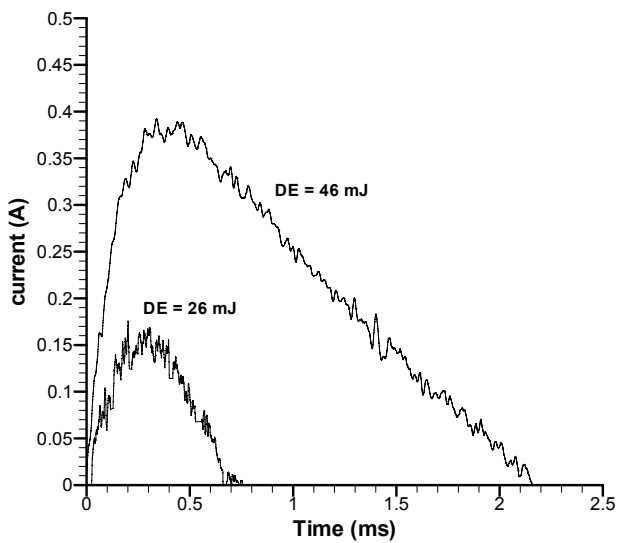
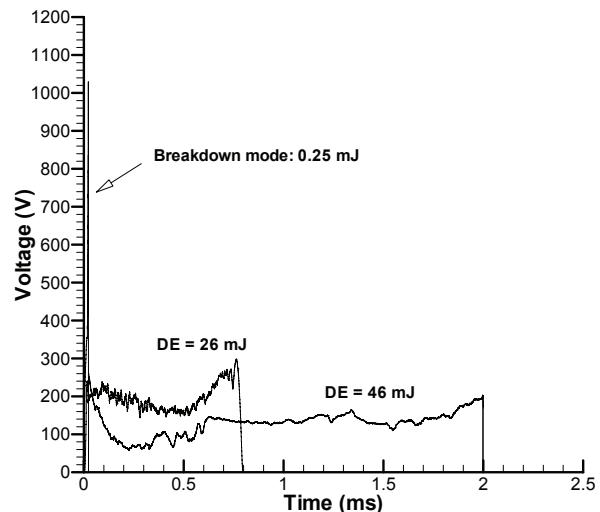


Figure 2: Voltage and current versus time for low and high discharge energies.

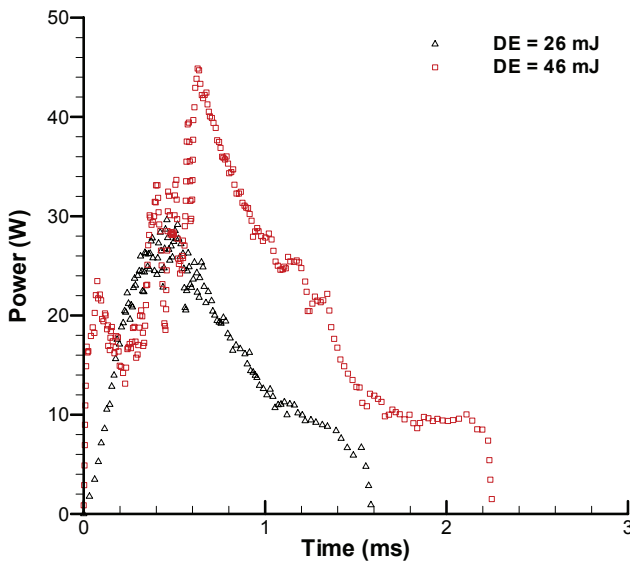


Figure 3: Spark discharge power of argon at low and high discharge energies.

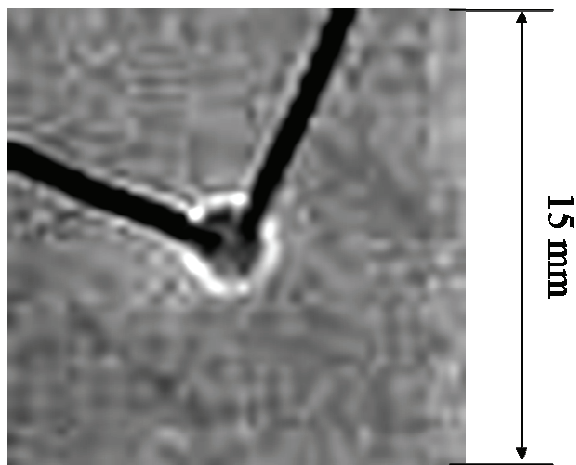


Figure 4: Argon plasma kernel, $P = 1 \text{ atm}$, $DE = 46 \text{ mJ}$.

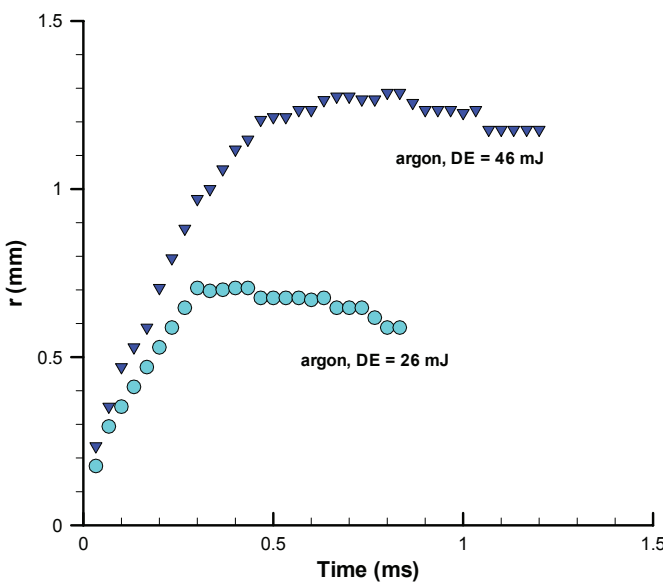


Figure 5: Argon radii at two different spark discharge energies ($DE = 26$ and 46 mJ).

4. Thermodynamic Model

In this section the thermodynamic model for predicting the growth of argon plasma kernel will be described. Figure 6 shows the schematic diagram of the control mass and energy transformation across the boundary.

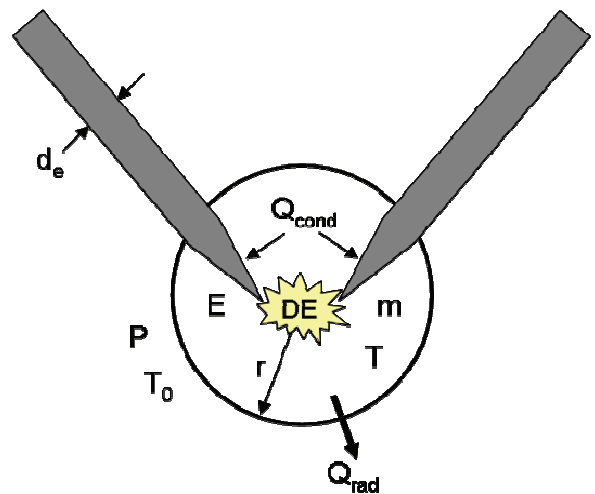


Figure 6: the sketch of the model.

The major assumptions are as following:

- 1- It is assumed that the plasma kernel is spherical.
- 2- All calculations start after the breakdown stage. It is assumed that the shock wave is emitted and pressure is constant.
- 3- Since the relaxation time scale of different energy modes (translational, rotational, vibrational, electronic) are too small ($O \sim 10^{-9} \text{ s}$), all species are in local thermodynamic equilibrium (Maly, 1981; Maly & Vogel, 1979; Sher et al, 1992; Sher & Keck, 1986).
- 4- There is no mass transport processes involved in the model. It is assumed that the plasma kernel is a constant-mass system and expands in a constant pressure process.
- 5- Energy losses are due to radiation, cathode-anode fall dissipations, and conduction through the thermal boundary layer to the electrodes.

The governing equations are, equation of state, mass conservation, and energy balance.

The equation of state is given as

$$pV = nRT \quad (1)$$

where p is the pressure, V is the volume of the kernel, n is number of moles, R is the universal gas constant, and T is the temperature. Total number of moles is determined by:

$$n = \sum_{i=1}^z n_i \quad (2)$$

where z is the number of species.

The number of elemental atom number is then given by

$$EA\epsilon = \sum_{\epsilon=0}^z Ar^{\epsilon} \quad \epsilon = 0, 1, 2, 3, \dots, z \quad (3)$$

In this equation, ϵ is the charge of ions.

The equation for energy balance is given by:

$$nc_v(T - T_0) = DE - p(\mathcal{V} - \mathcal{V}_0) - Q_{rad} - Q_{cond} \quad (4)$$

Eq. (4) can be rewritten as:

$$\frac{c_p}{R} p(\mathcal{V} - \mathcal{V}_0) = DE - Q_{rad} - Q_{cond} \quad (5)$$

where T is the temperature, c_v and c_p are the heat capacities, \mathcal{V}_0 is the initial volume of the kernel, Q_{rad} is the radiation energy loss, and Q_{cond} is the conduction energy loss to the electrodes through the thermal boundary layer. It should be noted that for each step the increment of temperature is chosen to be too small throughout the solution. This is the reason for integration of equations (4) and (5) versus temperature and appearance of constant specific heat capacities. It means that at each step it is assumed that the specific heat capacity is constant.

In Eqn. (5):

$$\begin{aligned} DE &= \int_0^b IVdt + \int_b^t (IV_{fall})dt + \int_b^t (IV_{col})dt \\ &= \int_0^b IVdt + Q_{ca} + SE \end{aligned} \quad (6)$$

In this equation, t is time, $\int_0^b IVdt$ is the breakdown energy, Q_{ca} is the cathode-anode fall dissipation by conduction into the electrodes, and SE is the net spark energy converted to thermal energy in the plasma.

Conduction to electrodes in the thermal boundary layer is:

$$Q_{cond} = 2 \int \frac{k_T A_e (T - T_0)}{\sqrt{\alpha t}} dt \quad (7)$$

where k_T is the thermal conductivity of the gas; A_e is the contact area of electrodes with the gas, T_0 is the temperature of the electrode, and α is the thermal diffusivity of argon.

Experimental data of Wilbers, Beulens, & Schram (2002), which have been collected at high temperatures under optically thin conditions, have been used to model radiation losses.

4.1. Thermodynamic properties: The thermodynamic properties of argon have been calculated by statistical thermodynamic methods. These parameters include c_p and the enthalpy of the mixture. For argon the species are Ar, Ar^+ , Ar^{2+} , Ar^{3+} , Ar^{4+} , Ar^{5+} , Ar^{6+} and e (electron). Additional information can be found in (Eisazadeh-Far, Metghalchi, & Keck, 2010). In the theoretical model, the values of specific heat are needed at very high temperatures of 300 – 100,000 K. Figure 7 shows the heat capacity of argon in this temperature range. Figure 8 shows the normalized number of species of argon. The results of Eq. (2) have been normalized by the sum of the elemental atom numbers defined in Eq. (3). It can be seen that number of particles increase as the temperature of the gas increases.

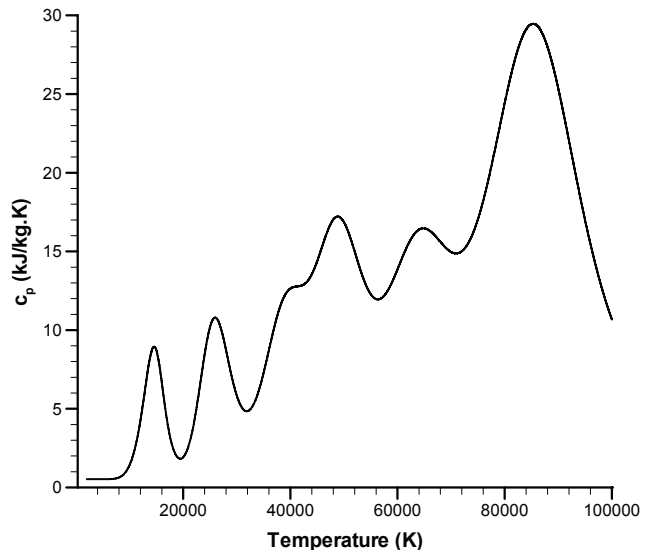


Figure 7: Specific heat capacity of argon at high temperatures.

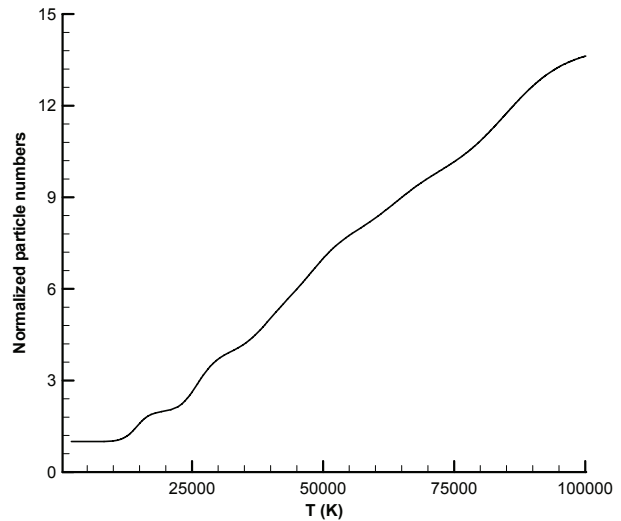


Figure 8: Particle numbers of argon normalized by elemental atom numbers.

5. Results and Discussion

Eqs. (1)–(7) have been solved to determine the radii and temperature of plasma kernel for different initial temperatures and volumes of the kernel and input electrical energies. The values of initial radius and initial temperature depend on the discharged energy, pressure, gas type and energy losses during the breakdown. The effect of initial parameters on the size and temperature of the kernel is investigated in the following Section.

5.1. Initial radius: Figures 9 and 10 demonstrate the effect of the initial radius of the plasma kernel on growth and temperature of the plasma kernel. It can be seen that the size of the plasma kernel is not dependent on the initial radius but the temperature of the kernel is very sensitive to the initial radius.

5.2. Initial temperature: Figures 11 and 12 show the effect of initial temperature on plasma kernel growth and its temperature. It is shown that initial temperature does not have a major effect on the size of the kernel but it can change the temperature of the hot plasma strikingly. Initial temperature depends on breakdown energy and breakdown

duration. The range of initial temperature for plasma is 5,000-7,000 K.

5.3. Best fit to the model: Figure 13 shows the results of the calculations and the comparison with the experimental data. There are two curves in each figure which are the calculations with and without radiation. As can be seen, radiation is a major source of energy loss. The radiation becomes important especially when the temperature is high. It can also be concluded that the decrease of argon plasma radii is due to radiation energy losses. At higher discharged energies not only the temperature of the kernel but also the

volume of kernel increases and it causes higher radiation energy losses.

Table 1 shows the summary of fractional energy terms. It can be seen that a large part of energy is dissipated by cathode-anode fall conduction dissipations. Clearly, the amount of radiation loss depends on the value of discharged energy. This percentage is strongly a function of the current and the temperature of the arc (Hermann & Schade, 1970). Table 2 shows that approximately 3-5 % of discharged energy is converted to thermal energy. The results presented in Table 1 are in good agreement with experimental measurements of Teets & Sell (1988).

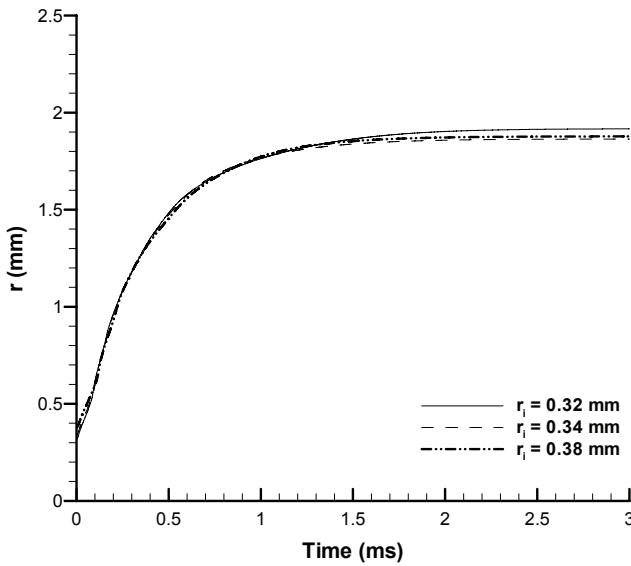


Figure 9: The effect of initial radius on kernel size of argon, $T_i = 7000$ K, DE = 46 mJ, $Q_{rad} = 0$.

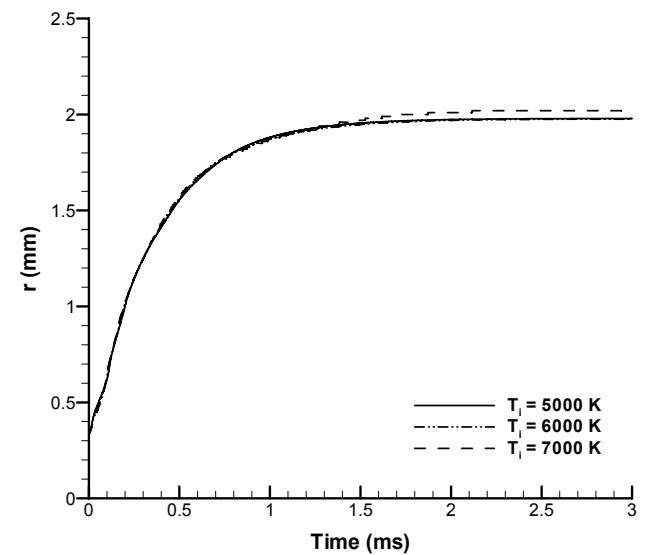


Figure 11: The effect of initial temperature on argon kernel growth, $T_i = 7000$ K, $r_i = 0.34$ mm, DE = 46 mJ, $Q_{rad} = 0$.

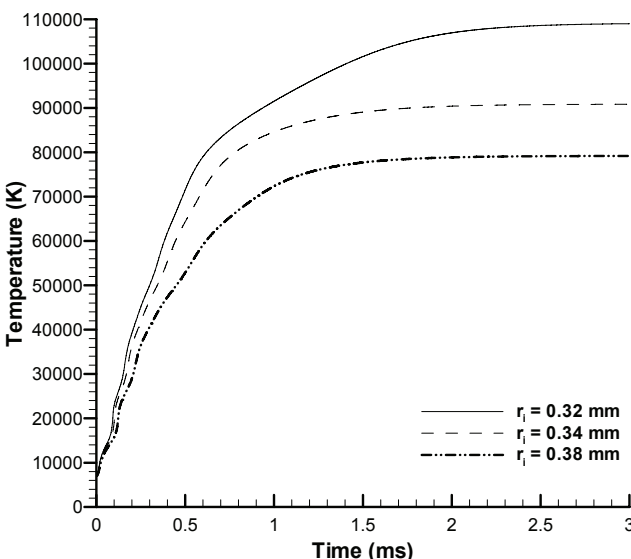


Figure 10: The effect of initial radius on kernel temperature of argon, $T_i = 7000$ K, DE = 46 mJ, $Q_{rad} = 0$.

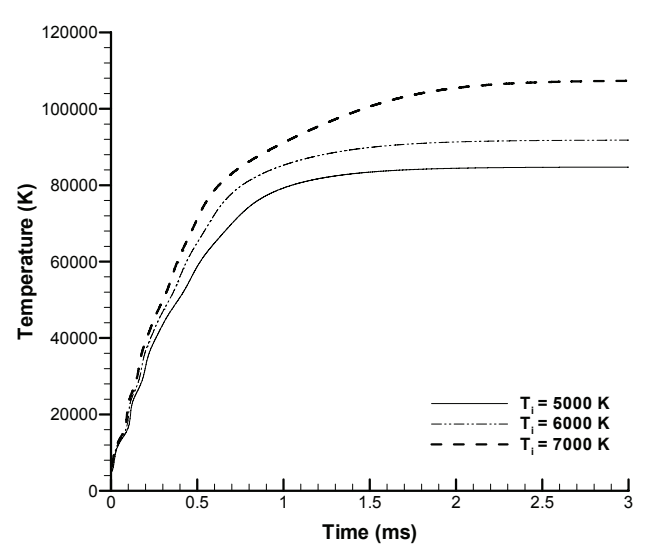


Figure 12: The effect of initial temperature on argon kernel temperature, $T_i = 7000$ K, $r_i = 0.34$ mm, DE = 46 mJ, $Q_{rad} = 0$.

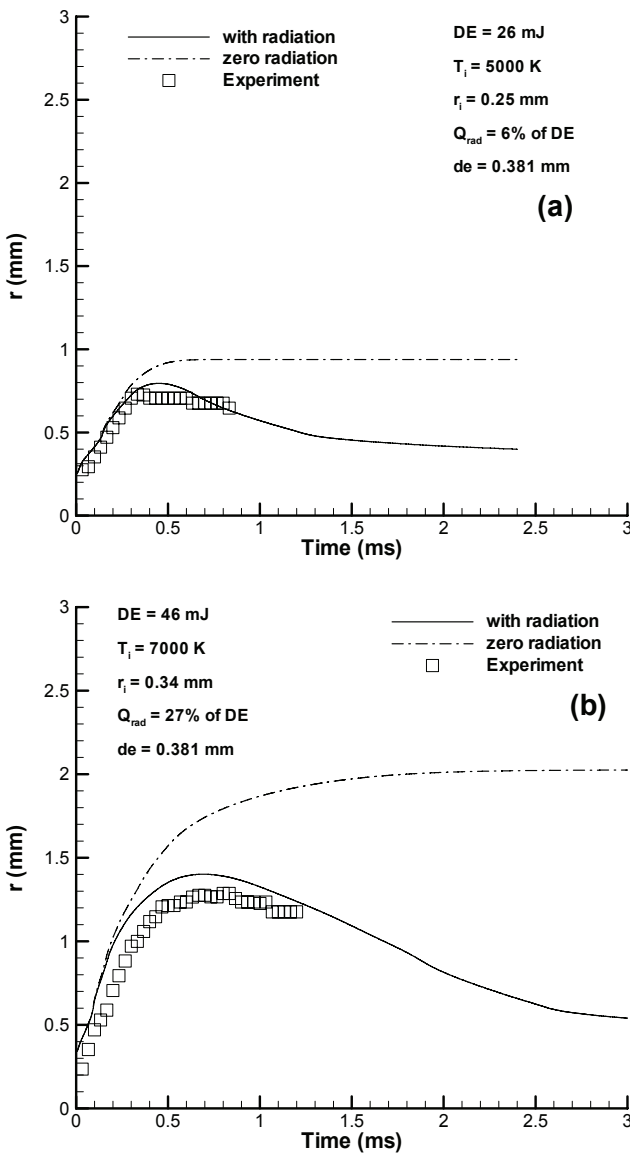


Figure 13: Argon plasma radii and comparison with experiments: a) DE = 26 mJ; b) DE = 46 mJ.

6. Conclusions

Formation of an argon plasma kernel has been studied experimentally and theoretically. The experiments were performed at constant pressure in a shadowgraph system. They have been performed with two different discharged energies to investigate the effect of spark energy. Radii of the argon plasma kernel were measured optically. A thermodynamic model was developed to predict the expansion of the kernel under initial conditions of experiments. The major conclusions are:

- 1- It can be assumed that the plasma kernel expands in a constant pressure and constant mass condition.

- 2- Total number of moles increases as the temperature of the gas increases and it is the main source of kernel expansion at constant pressure and constant mass condition.
- 3- Increase of heat capacity of the plasma gases at high temperatures plays a very important role on the temperature and growth mechanism of the kernel.
- 4- Initial volume and initial temperature of the kernel have a great effect on the temperature of the kernel. However, they do not have a major effect on the size of the kernel.
- 5- Cathode-anode falls are the major source of energy losses. Radiation is another source of energy losses which becomes more important at higher discharge energies due to higher kernel temperatures. A small portion of discharged energy is converted to thermal energy which depends on the discharged energy amount. This portion is less than 10%.
- 6- This model can be extended to combustible mixtures to investigate the spark ignition and flame formation mechanism of engines and other combustors.

Acknowledgment

This work has been partially supported by Office of Naval Research (ONR), grant number N00010-09-1-0479, under technical monitoring of Dr. Gabriel Roy.

References

- Bradley, D., Sheppard, C. G. W., Suardjaja, I. M., Woolley, R. 2004. *Fundamentals of high-energy spark ignition with lasers*, Combustion and Flame, 138(1-2), 55-77.
- Chen, Z., and Ju., Y. 2007. *Theoretical analysis of the evolution from ignition kernel to flame ball and planar flame*. Combustion Theory and Modeling, 11(3), 427 – 453.
- Eisazadeh-Far, K., Metghalchi, H., and Keck, J. C. 2010. *Thermodynamic Properties of Ionized Gases at High Temperatures*. Submitted to Journal of Energy Resources and Technology.
- Eisazadeh-Far, K., Moghaddas, A., Al-Mulki, J., Metghalchi, H. 2010. *Laminar Burning Speeds of Ethanol/Air/Diluent Mixtures*. Proc. Combust. Inst. (2010), doi:10.1016/j.proci.2010.05.105.
- Eisazadeh-Far, K., Parsinejad, F., and Metghalchi, H. 2010. *Flame structure and laminar burning speeds of JP-8/air premixed mixtures at high temperatures and pressures*. Fuel, 89, 1041–1049.
- Eisazadeh-Far, K., Parsinejad, F., Metghalchi, H., Keck, J. C. 2010. *On Flame Kernel Formation and Propagation in Premixed Gases*, Combustion and Flame, 157, 2211–2221.

Table 1: Summary of fractional energy terms

| | Argon (DE = 26 mJ) | Argon (DE = 46 mJ) |
|---|--------------------|--------------------|
| Cathode-anode fall losses | 88.80% | 68.20% |
| Thermal boundary layer conduction | 0.20% | 0.30% |
| Radiation losses | 6% | 27% |
| Converted to thermal energy (present study) | 5% | 3.50% |
| Converted to thermal energy (Teets and Sell (1988)) | 7% | |

- Hermann, W., Schade, E. 1970. *Transportfunktionen von Stickstoff bis 26000 K*. A. Physik. 233, 333-350.
- Kravchik, T., Sher, E. 1994. *Numerical modeling of spark ignition and flame initiation in a quiescent methane-air mixture*. Combustion and Flame, 99(3-4), 635-643.
- Lee, Y. G., Grimes, D. A., Boehler, J. T., Sparrow, J., Flavin, C. 2000. A Study of the Effects of Spark Plug Electrode Design on 4-Cycle Spark-Ignition Engine Performance, SAE Paper 2000-01-1210.
- Maly, R., Vogel, M. 1979. *Initiation and propagation of flame fronts in lean CH₄-air mixtures by the three modes of the ignition spark*. Symposium (International) on Combustion. 17(1), 821-831.
- Maly, R., 1981. *Ignition model for spark discharges and the early phase of flame front growth*. Symposium (International) on Combustion. 18(1), 1747-1754.
- Mantel, T. SAE Paper 920587.
- Parsinejad, F., Arcari, C., Metghalchi, H. 2006. *Flame Structure and Burning Speed of JP-10 Air Mixtures*. Combustion Science and Technology. 178, 975-1000.
- Parsinejad, F., Keck, J. C., and Metghalchi, H. 2007. On the location of flame edge in Shadowgraph pictures of spherical flames: a theoretical and experimental study. Experiments in Fluids. 43(6), 887-894.*
- Pischinger, S., Heywood, J. B. 1991. *A model for flame kernel development in a spark ignition engine*. Symposium (International) on Combustion. 23(1), 1033-1040.
- Rahim, F., Eisazadeh-Far, K., Parsinejad, F., Andrews, R. J., Metghalchi, H. 2008. *A Thermodynamic Model to Calculate Burning Speed of Methane-Air-Diluent Mixtures*, International Journal of Thermodynamics. 11, 151-161.
- Sher, E., Ben-Ya'Ish, J., Kravchik, T. 1992. *On the birth of spark channels*, Combustion and Flame, 89(2), 214-220.
- Sher, E., Keck, J. C. 1986. *Spark ignition of combustible gas mixtures*. Combustion and Flame. 66(1), 17-25.
- Teets, R. E., Sell, J. A. 1988. Calorimetry of Ignition Sparks, SAE Paper 880204.
- Wilbers, A. T. M., Beulens, J. J., Schram, D. C. 2002. *Radiative energy loss in a two-temperature argon plasma*, Journal of Quantitative Spectroscopy and Radiative Transfer, 46(5), 385-392.
- Yossefi, D., Belmont, R., Thurley, R., Thomas, J. C., Hacohen, J. 1993. *A Coupled Experimental-Theoretical Model of Flame Kernel Development in a Spark Ignition Engine*. SAE paper 932716.
- Ziegler, G. F. W., Wagner E. P., Maly, R. 1985. *Ignition of lean methane-air mixtures by high pressure glow and ARC discharges*, Symposium (International) on Combustion, 20(1), 1817-1824.